Corrosion inhibition of N80 steel simulated in an oil field acidification environment

Juan Du[1,], Jianhua Guo[2], Liqiang Zhao[1], Yixin Chen[1], Changlong Liu[1,3], Xianghai Meng[3]*

[1] School of Petroleum and Natural Gas Engineering, State Key Lab, Southwest Petroleum University, Chengdu, Sichuan 610500, P R of China;
[2] Engineering Technology Research Institute of Southwest Oil And Gas Field Company Petro china, Chengdu, Sichuan 610017, P R of China;
[3] CNOOC China Co. Ltd. Tianjin branch, Tianjin 300000, P R of China;
[*]E-mail: dujuanswpu@163.com

In this paper, the corrosion process of acidizing fluid (10% HCl + 8% HBF_4) in the production string was analyzed according to the acidizing procedure of the running pipe column. The amount of corrosion inhibitor, concentration of displacement fluid (NH_4Cl) and off-time (H) were investigated via an orthogonal design method to analyze the influence of the inhibition of acid corrosion of the immobile pipe string to confirm the main factors for corrosion of the oil tube. The results demonstrated that the amount of inhibitor was key to avoid corrosion of the immovable string by acidizing fluid. The corrosion and inhibition properties of N80 steel in fresh acid and residual acid solution were studied through electrochemical measurements and immersion tests. In addition, the corrosion morphology of the corrosion product was examined by scanning electron microscopy (SEM). The results showed that the N80 steel was more seriously corroded in the residual acid than in fresh acid. The pipe string also was corroded by the high-concentration acid liquid during acidification flow-back of the immobile pipe string. Therefore, effective measures should be taken to reduce corrosion due to residual acid on the pipe during the initial stage of acidizing flow-back.

1. INTRODUCTION

Recently, many oil fields have entered a recession, and stable utilization is becoming increasingly difficult. In addition, most original reservoir production is rapidly decreasing [1, 2]. Acid fracturing technology, a technology to improve oil production technology in oilfield development, is often used to improve oil production both at home and abroad [3, 4]. To reduce corrosion of the

production string by the acidizing fluid, most oilfields use acidizing operation of the pipe string [5-7]. The acidizing operation of a moving pipe column has a complicated construction process, long cycle and high construction cost. In particular, the construction of offshore platforms is affected greatly by the sailing date, and the platform occupies a large space. Therefore, the acidification of offshore platform acidizing primarily employs immobile pipe string acidizing [8].

Traditional mud acid (a mixed acid of hydrochloric acid and hydrofluoric acid (HF)) systems are considered effective matrix acids for removing silicate damage within 1 ft (0.3 m) of the wellbore [9, 10]. Applications of matrix acid to sandstone are increasing; in particular, the fluoroboric acid (HBF_4) system (8~15% HCl + 6~12% HBF_4) has been widely applied in oilfields [11-13]. However, this system can hydrolyze to produce HF in water and effectively penetrate deeply into sandstone during matrix acidizing operations, which ultimately will corrode metal equipment [14].

Compared to traditional acidification, original production string acidizing easily corrodes the tubing and equipment, including corrosion of the oil tube, case pipe, and submersible pump [15, 16]. Therefore, it is necessary to study the corrosion mechanism of matrix acidizing for steel to ensure the acidizing effect [17-19]. Great effort has been made to develop inhibitors for N80 steel in 15% HCl. There are many published reports of the inhibitory effects of different corrosion inhibitors, such as isatin compounds, synthesized hydrazine compounds, amino acid compounds, imidazoline compounds, pyrimidine derivatives, pyridine derivatives, chromenopyridin derivatives, benzimidazole derivatives, furfuryl alcohol, and benzyl quinolinium chloride [20-29]. Although researchers have discussed the effects of different corrosion inhibitors, these discussions have all focused on corrosion and corrosion inhibition of N80 steel in 15% HCl. Simulated corrosion of N80 steel in acidizing construction in the petroleum industry has not been discussed. Accordingly, the present study focused on corrosion and corrosion inhibition of N80 steel in acidizing construction.

In this work, static weight loss, potentiodynamic polarization curves, electrochemical impedance spectroscopy, surface morphology analysis and corrosion analysis were applied to study the corrosion behavior of N80 steel (an important steel in oil drilling) [30] placed in 10% HCl + 8% HBF_4, fresh acid (10% HCl + 8% HBF_4 + inhibitor), and spent acid (filtrates of fresh acid and reacted rock powder) respectively, and the anti-corrosion protection mechanism for N80 steel in this system. The results provide supporting information for the successful use of acidizing.

2. EXPERIMENT

2.1 Materials

Hydrochloric acid, NH_4Cl, tetrafluoroboric acid (HBF_4), ethanol and acetone of analytical reagent grade were purchased from Chengdu Kelon Chemical Reagent Company of China. The inhibitor was mainly composed of oleic-based imidazoline and thiourea (OIM : TU = 1 : 2), which were purchased from Chengdu Acidizing Petroleum Technology Development Co., Ltd.. Imidazoline (IM) and its derivatives have been identified as some of the most effective corrosion inhibitors for corrosion in the oil and gas industry [31, 32]. Therefore, IM and its derivatives have been widely used

in the oil and gas industry [33]. In this work, N80 steel specimens (50 mm × 10 mm × 3 mm) were used as received to investigate corrosive behavior; the chemical composition of the specimens is shown in Tab. 1. The 10% HCl + 8% HBF$_4$ solution was prepared by diluting the saturated HCl solution and 40% HBF$_4$ with deionized water. The rock debris was obtained from the reservoir of the Shahe formation in the PL19-3 oil field of Bohai, China, ground to form the powder particles, and used in the next experiment.
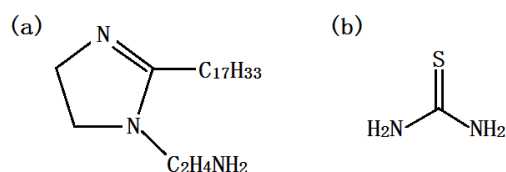
Figure 1. Structure of the oleic-based imidazoline (a) and thiourea (b).

Table 1. Chemical composition of N80 steel.

Alloy	C	Si	Mn	P	S	Cr	V	Al	Fe
Wt%	0.34	0.22	1.55	0.18	0.013	0.14	0.13	0.02	Bal.

Table 2. Preparation of acidizing fluid (spent acid was prepared under 333 k).

System	formula	Experimental target
Reference acid	10% HCl + 8% HBF$_4$	Reference experiments
Fresh acid	Reference acid + inhibitor	Simulate site acid
spent acid	The spent acid was filtered after a period of reaction with fresh acid and rock powder with a mass ratio of 10 to 1	Simulate site flow-back spent acid

Table 3. Main information about the spent acid.

System	content	elements
Solid content	1258 mg/L	O (52.27%), B (3.3%), Al (7.54%), Cl (6.91%), Ca (1.67%), Fe (8.56%), Si (17.59%), F (2.16%)
Liquid salinity	38453 mg/L	Fe (214 mg/L), Mg (138 mg/L), Ca (144 mg/L), Cl (2.82×10^4 mg/L), F (2200 mg/L), B (1100 mg/L)

2.2 Instruments

The following instruments were used: an HH-2K constant temperature water-bath (±0.1 ℃, Yuhua Instrument Company, Gongyi, China); ZF-9 electronic analytical balance (±0.1 mg, Shanghai Tetragonal Electronic Instrument Factory, China) [34]; CHI600 electrochemical workstation (Chenhua

Instrument Company, Shanghai, China); scanning electron microscope (SEM, JSM-7500F produced by JEOL); and X-ray diffractometer (XRD, X'Pert Pro MPD produced by Philips).

2.3 Experimental method

2.3.1 Corrosion experiment with the weight loss method

The fresh N80 steel was washed with acetone and ethyl alcohol, then dried in desiccators and accurately weighed. The N80 steel weight loss experiments were performed by immersing the steel in the reference acid, fresh acid and spent acid solution for different times and temperatures. The steel was immersed in acid solution using an HH-2K constant temperature water bath to control the temperature. Then, the N80 steel was removed, rinsed with deionized water, acetone and ethanol, dried in desiccators, and reweighed. The corrosion rate (C_R) was calculated using equation (1):

$$C_R = \frac{10^6 \Delta m}{St} \tag{1}$$

C_R ($g \cdot m^{-2} \cdot h^{-1}$) is the corrosion rate of each steel specimen, S (mm^2) is the surface area of the steel coupon, t (h) is the time of the corrosion reaction, and Δm (g) is the weight loss of the steel specimen. The corrosion inhibition efficiency (IE) of the corrosion inhibitor was calculated using equation (2):

$$IE = \frac{C_R - C_{Ri}}{C_R} \times 100 \tag{2}$$

C_R ($g \cdot m^{-2} \cdot h^{-1}$) and C_{Ri} ($g \cdot m^{-2} \cdot h^{-1}$) in equation (2) are the average corrosion rates in the absence and presence of inhibitor, respectively.

2.3.2 Electrochemical measurements

Polarization and electrochemical impedance spectroscopy (EIS) were used to investigate the corrosion behavior of N80 mild steel in acid solution, including reference acid, fresh acid and spent acid solution, in an electrochemical station with a three-electrode system at 333 K. The reference electrode, auxiliary electrode and working electrode used the standard chlorinated silver platinum electrode and N80 mild steel of 1 cm^2 (10 mm × 10 mm) [35], respectively. All potentials were measured versus SCE. All electrochemical measurements were obtained 30 min later (or longer) in acid solution, including reference acid, fresh acid and spent acid solution, after reaching a steady open circuit potential. Potentiodynamic polarization curves were obtained by changing the electrode potential automatically from -300 to +300 mV versus Eoc at a scan rate of 0.1 $mV.s^{-1}$. EIS measurements were obtained in a frequency range from 10^5 Hz to 10^{-2} Hz under potentiostatic conditions with an amplitude of 5 mV peak-to-peak using the AC signal at open circuit potential (Eoc) [36].

2.3.3 Surface analysis of N80 steel

The microstructure of the N80 steel surface immersed in acid solution, including reference acid, fresh acid and spent acid solution, was assessed by SEM. The elemental composition and content of corrosion products on the N80 steel surface were obtained using element mapping. The phase

composition of corrosion products on the N80 steel surface was evaluated by X-ray diffraction. The microstructure and elemental composition analysis were used to study the corrosion mechanism of N80 steel in the reference acid solution and the anti-corrosion mechanism of the corrosion inhibitor on N80 steel.

3. RESULTS AND DISCUSSION

3.1 Weight loss measurements

3.1.1 Acidizing experiments with primary and secondary factors of tubing corrosion

To study the primary and secondary factors of tubing corrosion, an acidizing experiment was conducted as follows. First, the fresh acid was prepared and injected into the oilfield well layer. The displacement fluid forces all acid in the wellbore to the well layer. Simultaneously, the well was shut for 1h to 3h with the existing displacement fluid. Finally, the spent acid generated from the fresh acid and the formation of a mineral reaction flowed back from the well layer and wellbore.

The orthogonal experiment was performed as follows. The simulation process of injection acid was conducted by immersing the N80 steel in fresh acid for 2 hours. Next, the simulated well was shut for the time of matrix acidizing for approximately 1 to 3 hours. The immersed steel was removed from the fresh acid and soaked in displacement fluid for hours. At the same time, the spent acid was prepared. The off-time is the difference between the acidizing time and the steel soaking time in the displacement fluid. Then, the spent acid flow-back process was simulated; that is, the soaked steel was removed from the displacement and immersed in the prepared spent acid for 3 hours (the time of flow-back is longer than the acid injection time). Finally, the impact of acidizing on tubing corrosion, including the concentration of inhibitor in the fresh acid and displacement fluid and the shut-in time, was assessed. The corrosion rate (C_R) was calculated based on the total time of acid reaction, which was approximately 5 hours.

The orthogonal design method was used to determine the primary and secondary factors of tubing corrosion for N80 steel subjected to acidizing. The impacts included the concentration of inhibitor in fresh acid and displacement fluid and the shut-in time. The levels and factors of the orthogonal experiment are shown in Tab. 4. There were 9 experiments according to the L9 (33) orthogonal table (Tab. 5). The different types of construction procedures in acidizing were simulated via the corrosion rates of N80 steel with different concentrations of inhibitor at 333 K, which is the same as the formation temperature of the Bohai PL19-3 oilfield. The results are shown in Tab. 5.

Table 4. Factors and levels of the orthogonal experiment for simulating the acidification environment.

Levels	factors		
	C_{inh} (wt%)	Displacement fluid	Shut-in time (h)
1	0.8	1.0% NH_4Cl	1.0
2	1.0	2.0% NH_4Cl	2.0
3	1.5	3.0% NH_4Cl	3.0

Table 5. Orthogonal experiment and results at 333 K.

Number	factors			$C_R / (g \cdot m^{-2} \cdot h^{-1})$	IE
	C_{inh} (wt%)	Displacement fluid	Shut-in time (h)		
1#	1	1	1	6.44	91.73
2#	1	2	2	6.48	91.71
3#	1	3	3	6.51	91.67
4#	2	1	2	5.62	92.79
5#	2	2	3	6.26	91.98
6#	2	3	1	6.00	92.32
7#	3	1	3	4.99	93.62
8#	3	2	1	5.35	93.13
9#	3	3	2	4.90	93.73
K_1	275.11	278.14	277.18		
K_2	277.09	276.82	278.23		
K_3	280.48	277.72	277.27		
k_1	91.70	92.71	92.39		
k_2	92.36	92.27	92.74		
k_3	93.49	92.57	92.42		
R	1.79	0.44	0.35		
Primary	$C_{inh} > C_{NH4Cl}$ B> Acid time				

Note: R is the value of extreme deviation; primary is the order of the effects of different influencing factors on the corrosion inhibition efficiency.

The results shown in Tab. 5 indicate that in the acidizing construction process, the main influencing factor for inhibiting tubing corrosion of N80 steel is the concentration of the inhibitor. Other impacts, such as the displacement fluid amount or the shut-in time, were not important factors for inhibiting tubing corrosion. Thus, to ensure success of the acidizing construction process, the oil tube, case pipe, submersible pump, and other equipment must be protected from corrosion by acid solutions. Therefore, an experiment with primary and secondary factors of tubing corrosion was designed. The results showed that the corrosion inhibitor is the key to tubing corrosion inhibition in an acidification environment. Previous reports have focused on oil well acidizing corrosion and inhibition in environments with high concentrations of HCl, such as 15% HCl [20-29, 37-39], without simulating the process of acidification. Imidazoline and thiourea are effective corrosion inhibitors in oil field environments, as reported by other researchers [40-43]. During the acidification of an oil well, fresh acid is injected into the formation for a short time under high pressure, but spent acid flow-back occurs due to the formation energy, and thus the spent acid can corrode the oil pipe for a long time. The data in Tab. 5 indicate that 0.8% inhibitor is sufficient to protect the tubing from corrosion in the acidizing construction process. The corrosion mechanisms of fresh acid and spent acid were also studied in the same experiment. The fresh acid consisted of 10% HCl + 8% HBF_4 + 0.8% inhibitor. The spent acid was the filtrates after reaction of fresh acid with rock powder for 2 hours, which is equivalent to the site shut-in time.

3.1.2 Effect of immersion time on the corrosion of N80 steel

The corrosion behavior of N80 steel and the stability of the inhibitor's inhibitory behavior were assessed on a time scale by weight loss measurements in reference acid solution, fresh acid, and spent acid solution for 2-10h at a temperature of 333 K.
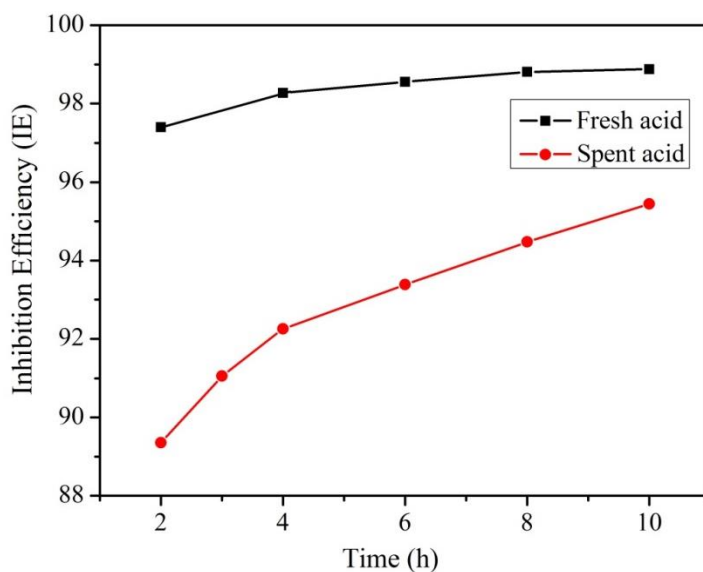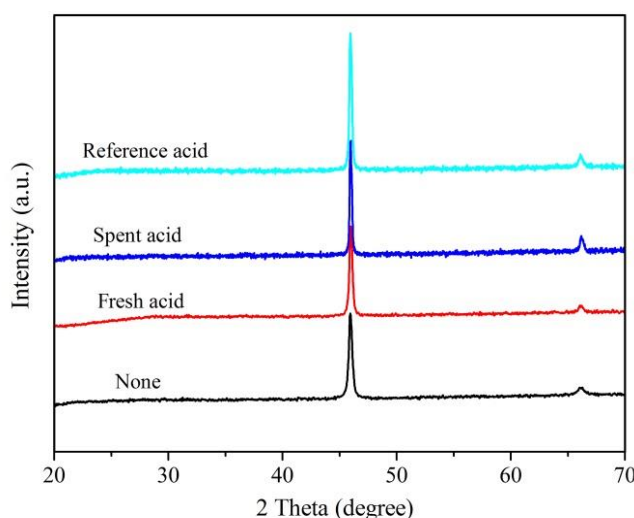

Figure 2. Influence of the immersion time of N80 on the inhibition efficiency in fresh acid (10% HCl + 8% HBF_4 + 0.8% inhibitor) and spent acid (filtrates of fresh acid and reacted rock powder) at 333 K.

As shown in Fig. 2, the IE was related to the soaking time. The IE increased in both fresh acid and spent acid with the soaking time for N80 steel, and the inhibition efficiency in fresh acid was better than that in spent acid. These results suggest that the acid injection process is not the cause of corrosion in the acidizing process; instead, spent acid flow-back is the true cause of corrosion. The spent acid is the product of the reaction between the fresh acid and formation minerals, and the concentration of this acid is lower than that of fresh acid. The results indicate that a portion of the inhibitors was adsorbed by the formation minerals after acid injection, resulting in a decrease in the concentration of the corrosion inhibitor. The IE of the fresh acid was greater than 97%, and no significant changes were observed in IE with increased soaking time. The stability of the inhibition efficiency implies that the inhibitor has long-term effects as an effective inhibitor. This stability may be due to the compact, complete protective layer formed on the steel surface, which plays a good protective role. Thus, the combination of imidazoline and thiourea requires a minimum soaking time in acid solution to form a stable surface film, similar to the results reported by Zou [40], Zhang [41] and Zhao [42]. According to the results of this experiment, the main reason for tubing corrosion in an oil field acidification environment is the spent acid, possibly because the rock debris adsorbs a portion of the inhibitor, thus decreasing the inhibitor concentration. The data in Fig. 2 show that the initial IE of the spent acid is low and that the IE improves with increasing soaking time. Thus, the results suggest that the corrosion of the pipe and equipment mainly occurred in the initial stage of acid flow-back.

Therefore, for acidizing, the corrosion of the pipe by the spent acid should be minimized in the early stage of acidizing flow-back. For example, in the early stage of flow-back, a sodium carbonate solution is neutralized in the air at the same time to neutralize the acid solution. Moreover, the reaction of sodium carbonate with the acid solution to produce CO_2 aid the flow-back of spent acid.

3.2 Analysis of the N80 steel surface and corrosion products

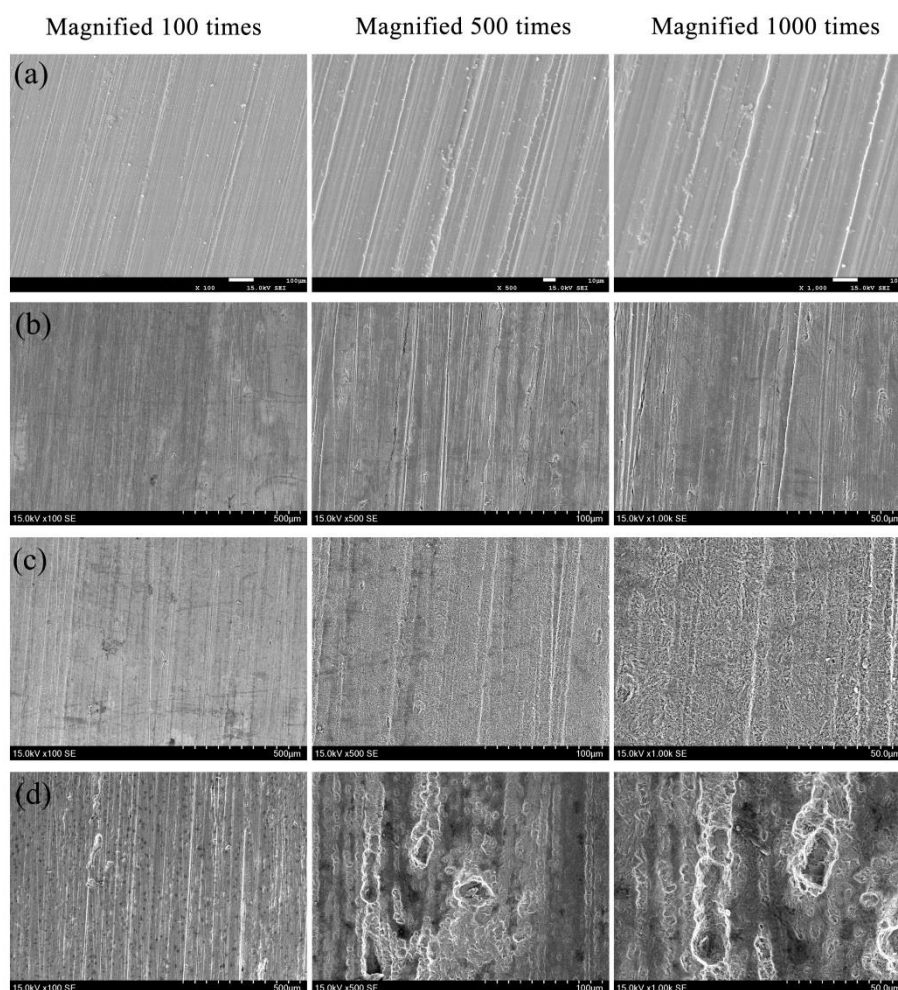**Figure 3.** X-ray diffraction pattern of N80 steel in reference acid (10% HCl + 8% HBF$_4$), fresh acid (10% HCl + 8% HBF$_4$ +0.8% inhibitor), and spent acid (filtrates of fresh acid and reacted rock powder).

X-ray diffraction (XRD) measurements were performed to investigate the phase composition of N80 steel and the corroded N80 steels that were immersed in the reference acid, fresh acid, and spent acid solutions. As shown in Fig. 3, the characteristic peaks of N80 steel are at 45.94 and 66.15, and the base line is relatively smooth. Compared with the characteristic peaks of N80 steel, the peaks of corrosive N80 steels did not obviously differ, but the intensities of the characteristic peaks of the corrosive N80 steel were gradually enhanced after immersion in fresh acid, spent acid and reference acid solution. In addition, the baseline of the immersed N80 steel fluctuated slightly due to corrosion of the steel; the corrosion products on the surface of the steel will generate some fluctuating signal peaks. The 4 XRD curves revealed no obvious changes in the characteristic peaks, indicating that the inhibitor inhibited the corrosion of N80 steel through dynamic physical and chemical adsorption, similar to the results reported by Zou [40], Zhang [41] and Zhao [42].

The microscopic morphologies and microstructure of the N80 steel and corroded N80 steels that were immersed in the reference acid, fresh acid, and spent acid solution were revealed using SEM, and the element distribution was determined by elemental mapping. The steel surface microphotographs at different magnifications are shown in Fig. 4. As shown in Fig. 4a, the polished N80 steel surfaces exhibited sequential streaks and a smooth profile. However, the N80 steel that was immersed in fresh acid was covered with corrosion products, and the surface was slightly corroded, as show Fig. 4b. For the steel immersed in spent acid, the surface featured less coverage with corrosion

products but greater corrosion; as a result, the surface was relatively blurred, and the streaks disappeared, as shown in Fig. 4c.

Figure 4. Scanning electron microscopy (SEM) image of the polished N80 steel surface (a) and N80 steel after immersion in fresh acid (10% HCl + 8% HBF$_4$ + 0.8% inhibitor) (b), spent acid (filtrates of fresh acid and reacted rock powder) (c), and reference acid (10% HCl + 8% HBF$_4$) (d).

When the N80 steel was immersed in reference acid solution in the absence of inhibitor, the steel surface appeared very rough due to the formation of uniform dot corrosion products on the steel surface. The surface was severely damaged, and many pits were visible in the microphotograph after removing the corrosion products on the steel surface. Imidazole and thiourea were easy to use as corrosion inhibitors in an acid environment to reduce mild pitting of steel, similar to the results reported by Zou [40], Zhang [44] and Xu [45]. These results suggest that the corrosion inhibitor generates a protective film, possibly due to adsorption of the inhibitor molecules on the steel surface. This film prevents attack of H$^+$ and Cl$^-$ on the steel metal surface. Although some pits were visible in microphotograph after removing the corrosion products on the steel surface, the number and diameter of the pits were greatly reduced on the surface with inhibitor compared with the surface without

inhibitor. To further investigate the elements in the layer covering the steel surface, the element distribution of the steel immersed in fresh acid was determined by elemental mapping, as shown in Fig. 5. Fe, Mn, and C were the main elements in the N80 steel, but a uniform distribution of O and Cl was also observed, indicating that the inhibitor molecules were absorbed on the steel surface to form the protective film. Thus, a combination of imidazoline and thiourea was dynamically adsorbed on the surface of the N80 steel, similar to the results reported by Zou [40], Zhang [41] and Zhao [42].
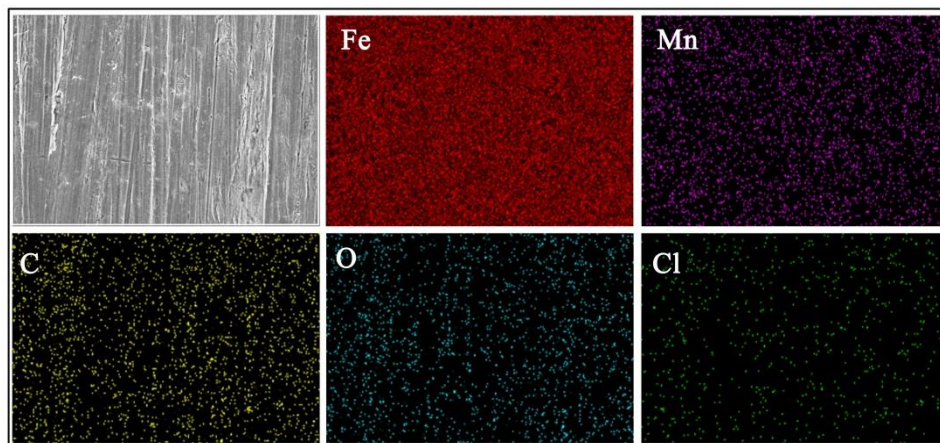

Figure 5. Elemental mapping images of N80 steel after immersion in fresh acid (10% HCl + 8% HBF$_4$ + 0.8% inhibitor).

3.3 Electrochemical measurements

The corrosion resistance of the N80 steel was investigated via the electrochemical impedance technique under different acid conditions. The impedance measurements and corrosion current density of the EIS experiment are presented in the form of Nyquist plots and polarization curves. The N80 steel was soaked in reference acid, fresh acid and spent acid. Before electrochemical testing, the samples were immersed in different acid solutions for 60 min to obtain a stable open-circuit electrode. As shown in Fig. 6, the arc radius on the EIS Nyquist plot of N80 steel in fresh acid solution was greater than that for N80 steel in reference acid and spent acid solution, and the impedance of the spent acid was greater than that of the reference acid. These results suggest that the inhibitor can be adsorbed on the surface of the steel to form a protective film, which improves the impedance value and prevents the acid solution from corroding the steel. The EIS plot measured in reference acid is interpreted by the equivalent electric circuit shown in Fig. 7a, and the EIS plots measured in fresh acid and spent acid are interpreted by the equivalent electric circuits shown in Fig. 7b. The corresponding electrochemical parameters are given in Tab. 6. R_s is the solution resistance; R_{ct} represents the charge transfer resistance, and CPE is the constant phase element. The R_s of the spent acid was much higher than those of the reference acid and the fresh acid, which may be due to the large amount of rock particles in the spent acid. The $R_{ct1} + R_{ct2}$ of fresh acid and spent acid was far higher than the R_{ct} of reference acid, which suggests that the corrosion inhibitor inhibited charge transfer of N80 corrosion. The charge transfer resistance indicates that the inhibitor formed a thin protective layer on the steel surface, thus preventing and slowing the corrosion reaction. The charge transfer resistance of the spent acid was

lower than that of fresh acid, possibly because the rock debris adsorbed a portion of the corrosion inhibitor in the spent acid and thus decreased the inhibitor layer thickness. The equivalent electric circuit demonstrates that the inhibitor is an effective mixed-type corrosion inhibitor. Similar results have been reported by other researchers [40-43,46].

 To further confirm the results, the corrosion current density of steel was investigated using electrochemical station test polarization curves of N80 steel under different acid conditions. As shown in Fig. 8, the corrosion potential of the reference acid was more negative, facilitating steel corrosion. Related electrochemical parameters are listed in Tab. 7. Compared with the spent acid, the fresh acid decreased the corrosion current densities and increased the inhibition efficiency (η%). The inhibition efficiencies of fresh acid and spent acid were 89.78% and 83.66%. Therefore, in the acidizing process, the main factor causing corrosion of the tube is spent acid. The combination of imidazoline and thiourea can effectively inhibit the corrosion of the pipe during oil well acidizing, similar to reports by other researchers [40-46]. Thus, all types of corrosion inhibitors can effectively inhibit the corrosion of the pipe when the oil well is injected with acid.
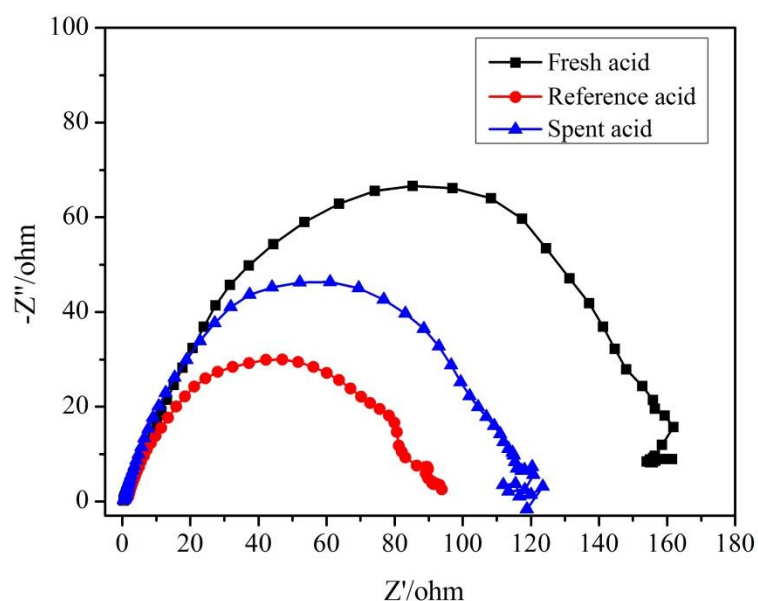
Figure 6. Nyquist curves for N80 steel immersed in reference acid (10% HCl + 8% HBF$_4$), fresh acid (10% HCl + 8% HBF$_4$ + 0.8% inhibitor), and spent acid (filtrates of fresh acid and reacted rock powder) at 333 K.
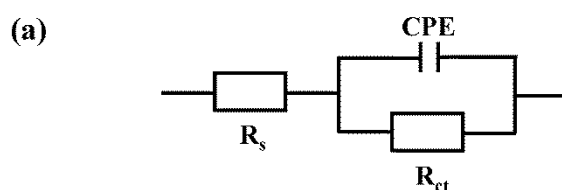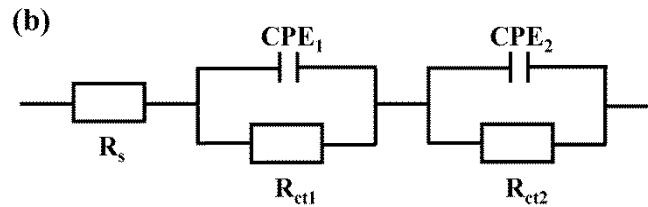
Figure 7. Equivalent electric circuit diagram used to fit the EIS data for (a) reference acid (10% HCl + 8% HBF$_4$), (b) fresh acid (10% HCl + 8% HBF$_4$ + 0.8% inhibitor) and spent acid (filtrates of fresh acid and reacted rock powder).

Table 6. Equivalent circuit parameters of EIS results at 333 K.

System	R_s $(\Omega\ cm^2)$	R_{ct1} $(\Omega\ cm^2)$	Q_1 $(\Omega^{-1}\ cm^{-2}\ s^n)$	n_1	R_{ct2} $(\Omega\ cm^2)$	Q_2 $(\Omega^{-1}\ cm^{-2}\ s^n)$	n_2
reference acid	0.2440	-	-	-	94.57	9.464×10^{-5}	0.6946
Fresh acid	0.2522	19.49	8.367×10^{-4}	0.8269	142.9	1.974×10^{-4}	0.9083
Spent acid	0.3892	0.4752	1.564×10^{-5}	0.8000	117.1	1.211×10^{-4}	0.8277
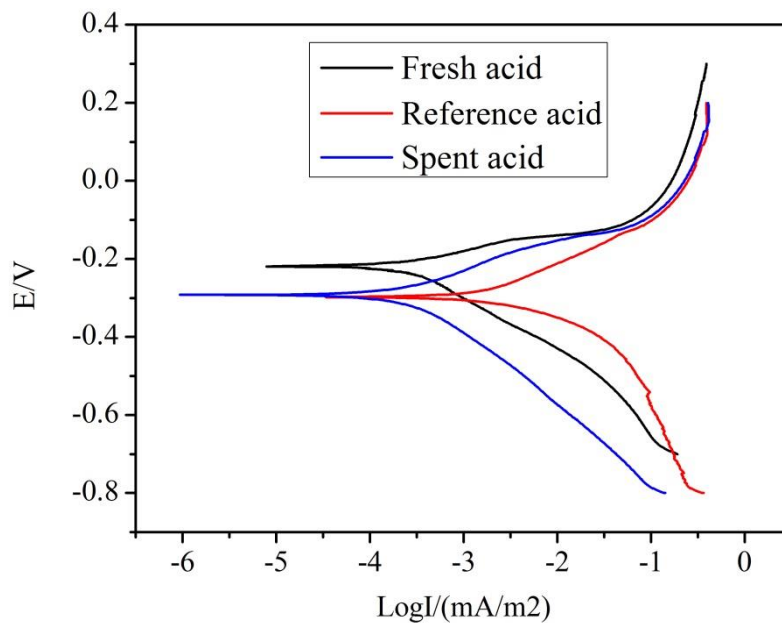
Figure 8. Polarization curves for N80 steel immersed in reference acid (10% HCl + 8% HBF$_4$), fresh acid (10% HCl + 8% HBF$_4$ + 0.8% inhibitor), and spent acid (filtrates of fresh acid and reacted rock powder) solution at 333 K.

Table 7. Electrochemical parameters of the polarization curves at 333 K.

System	E_{corr} (mV)	i_{corr} (A/cm^2)	IE%
reference acid	-292	1.83×10^{-3}	-
Fresh acid	-213	1.87×10^{-4}	89.78%
Spent acid	-280	2.99×10^{-4}	83.66%

4. CONCLUSION

In summary, the corrosion behavior of N80 steel was investigated by orthogonal experiments in 10% HCl + 8% HBF$_4$, fresh acid and spent acid solution. The corrosion morphology and behavior were studied using SEM and an electrochemical station. The results showed that the N80 steel was more seriously corroded in the residual acid than in fresh acid. This result is primarily due to adsorption of the corrosion inhibitor in acid solution by the reservoir formation minerals during reservoir acidification; the flow-back electrolyte from the formation accelerates the corrosion of the pipe string by the residual acid. Therefore, relevant measures should be taken to avoid residual acid corrosion on the pipe during the initial stage of acidizing flow-back.

References

1. Y. Lv, Y. Wang, *Pet. Ttubular Goods Instrum.*, 1 (2015) 5.
2. C. Li, *Surf. Technol.*, 45 (2016) 80.
3. Z. Qu, N. Qi, Z. Wang, *Pet. Geol. Rec. Effic.*, 13 (2006) 93.
4. S. Zhou, X. Guo, S. Du, *Corros. Sci. Prot. Technol.*, 26 (2014) 469.
5. E. D. Franceschi, T. Castiñeiras, F. Benedetto, A. Funes, F. Figini, M. J. Economides, *J. Nat. Gas Sci. Eng.*, 12 (2013) 65.
6. S. Zhu, J. Wei, Z. Bai, G. Zhou, J. Miao, R. Cai, *Eng. Fail. Anal.*, 18 (2011) 950.
7. C. Zhang, Z. Tie, X. Cao, D. Chen, *Nat. Gas Ind. B,* 3 (2016) 563.
8. X. Li, G. Zhang, J. Ge, D. Ma, N. Qi, H. Wu, *J. Nat. Gas Sci. Eng.*, 35 (2016) 11.
9. R. Abdollahi, S. R. Shadizadeh, *Sci. Iran.*, 6 (2012) 1665.
10. M. N. Al-Dahlan, H. A. Nasr-El-Din, A. A. Al-Qahtani, *Soc. Pet. Eng.*, 65032 (2001) 1.
11. K. R. Kunze, C. M. Shaughnessy, *Soc. Pet. Eng. J.,* 1 (1983) 65.
12. M. U. Shafiq, M. T. Shuker, *Soc. Pet. Eng.*, 169641 (2013) 1.
13. H. Nasr-El-Din, L. Zhou, *Soc. Pet. Eng.*, 164050 (2013) 1.
14. M. Finšgar, J. Jackson, *Corros. Sci.*, 3 (2014) 17.
15. Y. Z. Li, N. Xu, X. P. Guo, G. A. Zhang, *Corros. Sci.*, 126 (2017) 127.
16. L. Wei, X. Pang, M. Zhou, K. Gao, *Corros. Sci.*, 121 (2017) 57.
17. A. M. Atta, G. A. El-Mahdy, A. K. F. Dyab, H. A. Allohedan, *Int. J. Electrochem. Sci.,* 7 (2013) 9629.
18. C. Wang, Y. Li, W. Zhou, *Int. J. Electrochem. Sci.,* 6 (2016) 4399.
19. Y. Hu, Y. Peng, W. Zhang, M. Song, *Int. J. Electrochem. Sci.,* 5 (2017) 4360.
20. M. Yadav, U. Sharma, P. N. Yadav, *Egypt. J. Pet.*, 3 (2013) 335.
21. M. Yadav, D. Sharma, T. K. Sarkar, *J. Mol. Liq.*, 212 (2015) 451.
22. M. Yadav, T. K. Sarkar, T. Purkait, *J. Mol. Liq.*, 212 (2015) 731.
23. M. Yadav, D. Behera, U. Sharma, *Arab. J. Chem.*, 4 (2016) 1487.
24. J. Haque, K. R. Ansari, V. Srivastava, M. A. Quraishi, I. B. Obot, *J. Ind. Eng. Chem.*, 49 (2017) 176.
25. K. R. Ansari, M. A. Quraishi, A. Singh, *Measurement*, 76 (2015) 136.
26. K. R. Ansari, M. A. Quraishi, A. Singh, *J. Assoc. Arab Univ. Basic. Appl. Sci.*, 22 (2015) 45.

27. M. Yadav, S. Kumar, T. Purkait, L. O. Olasunkanmi, I. Bahadur, E. E. Ebenso, *J. Mol. Liq.*, 213 (2016) 122.
28. S. Vishwanatham, N. Haldar, *Corros. Sci.*, 11 (2008) 2999.
29. Z. Yang, F. Zhan, Y. Pan, Z. LYu, C. Han, Y. Hu, P. Ding, T. Gao, X. Zhou, Y. Jiang, *Corros. Sci.*, 99 (2015) 281.
30. A. M. Atta, G. A. El-Mahdy, H. A. Allohedan, S. M. El-Saeed, *Int. J. Electrochem. Sci.,* 10 (2015) 8.
31. M. Heydari, M. Javidi, *Corros. Sci.*, 61 (2012) 148.
32. K. Zhang, B. Xu, W. Yang, X. Yin, Y. Liu, Y. Chen, *Corros. Sci.*, 90 (2015) 284.
33. Y. Z. Li, N. Xu, G. R. Liu, X. P. Guo, G. A. Zhang, *Corros. Sci.*, 112 (2016) 426.
34. Y. Zhu, J. Zhuang, X. Zeng, *Appl. Surf. Sci.*, 313 (2014) 31.
35. W. Cui, L. Tian, Zhao, Y. Zhi, G. Xiao, W. Da, *Int. J. Miner., Metall. Mater.*, 23 (2016) 176.
36. K. R. Ansari, Sudheer, A. Singh, M. A. Quraishi, *J. Dispersion Sci. Technol.*, 7 (2015) 908.
37. E. B. Ituen, O. Akaranta, S. A. Umoren, *J. Mol. Liq.*, 246 (2017) 112.
38. S. A. Haladu, S. A. Umoren, S. A. Ali, M. M. Solomon, *Int. J. Electrochem. Sci.,* 10 (2017) 9061.
39. M. Yadav, D. Sharma, S. Kumar , *Korean J. Chem. Eng.*, 5 (2015) 993.
40. Y. Zuo, L. Yang, Y. Tan, Y. Wang, J. Zhao, *Corros. Sci.*, 120 (2017) 99.
41. J. Zhang, X. L. Gong, H. H. Yu, M. Du, *Corros. Sci.*, 10 (2011) 3324.
42. J. Zhao, G. Chen, *Electrochim. Acta*, 5 (2012) 247.
43. L. Guo, S. Kaya, I. B. Obot, X. Zheng, Y. Qiang, *J. Colloid Interface Sci.,* 2 (2017) 478.
44. L. Zhang, Y. He, Y. Zhou, R. Yang, Q. Yang, *Petrol.*, 3 (2015) 237.
45. B. Xu, W. Gong, K. Zhang, W. Yang, Y. Liu, X. Yin, H. Shi, Y. Chen, *J. Taiwan Inst. Chem. Eng.,*
46. I. Ullah, M. Khan, A. Shah, S. Z. Khan, *Tenside, Surfactants, Deterg.*, 6 (2017) 510.